RESEARCH PAPER

Theoretical solution for drained cylindrical cavity expansion in clays with fabric anisotropy and structure

Jorge Castro[1] · Nallathamby Sivasithamparam[2]

Abstract

This paper presents a novel, exact, semi-analytical solution for the quasi-static drained expansion of a cylindrical cavity in soft soils with fabric anisotropy and structure. The assumed constitutive model is the S-CLAY1S model, which is a Cam clay-type model that considers fabric anisotropy that evolves with plastic strains, structure and gradual degradation of bonding (destructuration) due to plastic straining. The solution involves the numerical integration of a system of eight first-order ordinary differential equations, three of them corresponding to the effective stresses in cylindrical coordinates, other three corresponding to the components of the fabric tensor and one corresponding to the amount of bonding and another corresponding to the specific volume. The solution is validated against finite element analyses. When destructuration is considered, the solution provides slightly lower values of the effective radial and mean stresses near the cavity wall. Besides, the specific volume is further reduced due to loss of bonding. Parametric analyses and discussion of the influence of soil overconsolidation, expansion of the cavity and initial amount of bonding are presented.

Keywords Bonding · Cavity expansion · Clays · Destructuration · Fabric of soils · Theoretical analysis

List of symbols

a	Radius of the cylindrical cavity
D	Elastic stiffness matrix
e	Void ratio
f_y	Function of the yield surface
G	Shear modulus
K_0	Coefficient of lateral earth pressure at rest
M	Slope of the critical state line
p'	Mean effective stress: $p' = \frac{(\sigma'_r + \sigma'_\theta + \sigma'_z)}{3}$
p'_m	Size of the yield surface
p'_{mi}	Size of the intrinsic yield surface
q	Deviatoric stress: $q = \sqrt{\frac{1}{2}\left(\sigma'_r - \sigma'_\theta\right)^2 + \left(\sigma'_r - \sigma'_z\right)^2 + \left(\sigma'_\theta - \sigma'_z\right)^2}$
$\overline{q}$	Invariant for anisotropic models. Radius of the yield surface in π-plane
Q	Invariant for anisotropic models: $Q = \frac{2}{3}\overline{q}^2$
S_t	Sensitivity
s	Deviatoric stress
u_r	Radial displacement
$\boldsymbol{\alpha}$	Fabric tensor
α	Inclination of the yield surface
$\boldsymbol{\alpha_d}$	Deviatoric fabric tensor
Δ	Incremental operator
Λ	Plastic multiplier
ε	Strain
η	Stress ratio: $\eta = q/p'$ or $\boldsymbol{\eta} = \boldsymbol{\sigma_d}/p'$ (tensor)
κ	Slope of swelling line from $v - \ln p'$ space
λ	Slope of the natural post-yield compression line from $v - \ln p'$ space
λ_i	Slope of the intrinsic yield compression line from $v - \ln p'$ space
v	Poisson's ratio
ξ	Auxiliary variable for the radial position $\xi = \frac{u_r}{r} = \frac{r - r_0}{r}$

Bold notation is used for tensors.
Compressive stresses and strains are assumed as positive because it is the conventional sign notation in geotechnical engineering.

✉ Jorge Castro
castrogj@unican.es

Nallathamby Sivasithamparam
nallathamby.siva@ngi.no

1 Group of Geotechnical Engineering, Department of Ground Engineering and Materials Science, University of Cantabria, Avda. de Los Castros, s/n, 39005 Santander, Spain

2 Computational Geomechanics Division, Norwegian Geotechnical Institute, Oslo, Norway

🌐 Springer

ξ, ξ_d	Absolute and relative effectiveness of plastic strains in destructuration
σ, σ'	Total and effective stresses
σ_a	Internal cavity pressure
σ'_p	Effective radial stress at the elastic/plastic boundary
υ	Specific volume
χ	Bonding parameter
ω, ω_d	Absolute and relative effectiveness of rotational hardening

Abbreviations

CS	Critical state
CSL	Critical state ratio
YS	Yield surface

Subscripts/superscripts

0	Initial
d, v	Deviatoric, volumetric
H, V	Horizontal, vertical
i	Any of the axis components r, θ, z
p	Plastic
r, θ, z	Cylindrical coordinates

1 Introduction

Cavity expansion theory has been applied widely in geotechnical problems (e.g. [24, 25, 38]). Analytical solutions cover both cylindrical and spherical cavities, expansion from a null or finite initial radius, undrained or drained conditions and different types of material constitutive models (e.g. [43]). Chen and Abousleiman [7] developed a rigorous semi-analytical solution for the undrained expansion of a cylindrical finite cavity in a modified Cam clay (MCC) material. The solution is rigorous because it is developed without any approximation imposed on the mean and deviatoric stresses and it is semi-analytical because it requires the numerical integration of a system of three first-order ordinary differential equations, corresponding to the effective stresses in cylindrical coordinates. Vrakas [39] has later presented a more general solution for the undrained cylindrical cavity expansion, considering any type of two-invariant model belonging to the critical state (Cam clay) family, using large strain formulation also in the elastic zone and reducing the numerical procedure to a single nonlinear equation.

Chen and Abousleiman [8] extended their previous solution [7] to drained conditions. The extension is non-trivial because the volumetric strain is no longer null and must be considered as an additional variable in combination with the effective stresses. The distinctive feature of Chen and Abousleiman [8] is the ingenious introduction of an auxiliary variable that is the ratio of the particle displacement in the radial direction to its present radial position ($\xi = u_r/r$). Thus, the solution for drained conditions requires adding a partial differential equation for the specific volume (υ) and using the auxiliary variable (ξ) instead of the radial coordinate (r).

Chen and Abousleiman [7, 8] solutions have opened the path for semi-analytical solutions for anisotropic critical state plasticity models, and it is a subject currently undergoing intense study [5, 6, 9, 10, 18–22, 34, 44]. These anisotropic solutions add three partial differential equations to the system, corresponding to the fabric tensor. All these anisotropic models assume isotropic elasticity for simplicity. Models that consider anisotropic elasticity (e.g. [4, 29] are beyond the scope here. Table 1 summarizes the main features of the solutions that follow the Chen and Abousleiman [7, 8] approach for the cylindrical cavity expansion problem and are directly related to the proposed solution here. Sivasithamparam and Castro [34] showed that the rotational hardening law must be considered to obtain realistic results, and Chen et al. [10] discussed the benefits of using a rotational hardening law that predicts a

Table 1 Summary of semi-analytical cavity expansion solutions directly related to the proposed solution

Type of constitutive model	Model name and reference	Undrained solution	Drained solution
Isotropic critical state	MCC	Chen and Abousleiman [7]	Chen and Abousleiman [8]
Anisotropic without rotational hardening	K_0-AMCC [36]	Li et al. [20]	Li et al. [19]
Anisotropic with rotational hardening by plastic volumetric strains	Dafalias [11, 12]	Chen and Liu [9]	Liu and Chen [21]
	AMCC model with SMP criterion [42]	Chen et al. [5]	
Anisotropic with rotational hardening by both volumetric and deviatoric plastic strains	S-CLAY1 [40]	Sivasithamparam and Castro [34]	Chen et al. [6]
Fabric anisotropy and structure	S-CLAY1S [16]	Sivasithamparam and Castro [35]	Proposed solution

unique critical state as done by Sivasithamparam and Castro [34], using the SCLAY1 [40] model for the cylindrical cavity expansion problem.

The authors [35] have recently developed a theoretical solution that considers fabric anisotropy and structure using the S-CLAY1S constitutive model [16] for undrained conditions. Using a constitutive model that considers soil structure and gradual degradation of bonding (destructuration) allows reproducing the strength loss in sensitive clays (e.g. immediately after pile driving) [35]. This paper presents the corresponding solution for drained conditions using the auxiliary variable proposed by Chen and Abousleiman [8]. Although solutions for cavity expansion in isotropic strain-softening soils (e.g. [24]) and interpretation of pressuremeter tests in sensitive soils (e.g. [17, 30, 31]) using a post-failure strain softening had been presented, the authors' solutions are the first ones for anisotropic, structure (inter-particle bonding) and destructuration behaviour of plastic nature of clays. It is worth noting that neglecting soil structure leads to inaccurate predictions of clay responses under external loading (e.g. [3, 13, 15, 27, 28]).

In this way, this paper presents a novel, exact and semi-analytical cylindrical cavity expansion solution for drained conditions and for natural clays, which exhibit fabric anisotropy and structure. The solution is developed using the S-CLAY1S constitutive model [16], which considers fabric anisotropy that evolves with plastic strains, structure and gradual degradation of bonding (destructuration) due to plastic straining. In cavity expansion problems, real situations are commonly close to the undrained case for clays, but depending on the rate of loading and the soil permeability, the behaviour may be partially drained (e.g. [15]). For these cases, the proposed drained solution sets the other limit values.

The assumptions and mathematical derivation of the semi-analytical solution are presented in Sect. 2. A system of eight first-order ordinary differential equations that require numerical integration is obtained. Details of the mathematical formulation are included as separate appendixes for simplicity and clarity. Validation of the semi-analytical solution against finite element analyses, results and parametric analyses are portrayed in Sect. 3. The solution allows to obtain the increase in the cavity pressure with the radial expansion of the cavity and variations of stresses, specific volume, fabric anisotropy and amount of bonding around the cavity (Sect. 3). Besides, the stress paths at the cavity wall are also presented in Sect. 3. Finally, the main conclusions are summarized in Sect. 4.

2 Mathematical formulation and semi-analytical solution

### 2.1 Assumptions and basic equations

The following assumptions are made to simplify the study of the quasi-static expansion of a cylindrical cavity of initial radius a_0 under drained conditions:

1. The axis of the cylindrical cavity is assumed as the vertical axis, and the initial stress state is homogeneous and consists of a horizontal effective stress and a vertical effective stress (σ'_H, σ'_V).
2. The soil has an initial uniform void ratio ($e_0 = \upsilon_0 - 1$).
3. The pore water pressure is always equal to its initial hydrostatic value (u_0); consequently, its value is irrelevant for the solution. For the sake of simplicity, its value is assumed as 0 here, and effective and total stresses are the same ($\sigma_H = \sigma'_H, \sigma_V = \sigma'_V$).
4. The initial horizontal stress on the cavity is also σ_H, and it increases up to σ_a, upon expanding the cavity to a final radius a (Fig. 1).
5. Soil behaviour is reproduced using the S-CLAY1S constitutive model [16], which assumes isotropic elasticity.
6. The symmetry axis of the initial soil plastic cross-anisotropy (transversely isotropic material) is the vertical one. This ensures that the cavity keeps as a cylinder and does not change to an elliptic shape (e.g. [45]).
7. The problem has axial symmetry; thus, shear stresses vanish and, due to the infinite extent of the soil, plane strain conditions hold.
8. Cylindrical coordinates (r,θ,z) are used throughout the paper because they are principal directions for this problem. Principal effective stresses are radial σ'_r, tangential σ'_θ and vertical σ'_z.
9. Large strain deformation is considered in the plastic region using natural (or logarithmic) strains, but small-strain deformation is used in the elastic region.

The last simplifying assumption has a negligible influence on the results because in the elastic region, the strains are much smaller than those in the plastic annulus. For example, Vrakas [39] presented a solution that considers large strains also in the elastic zone, and the differences are insignificant.

The equilibrium equation in the radial direction for cylindrical coordinates, which are principal directions, using effective stresses may be written as

$$\frac{\partial \sigma'_r}{\partial r} + \frac{\sigma'_r - \sigma'_\theta}{r} = 0 \tag{1}$$
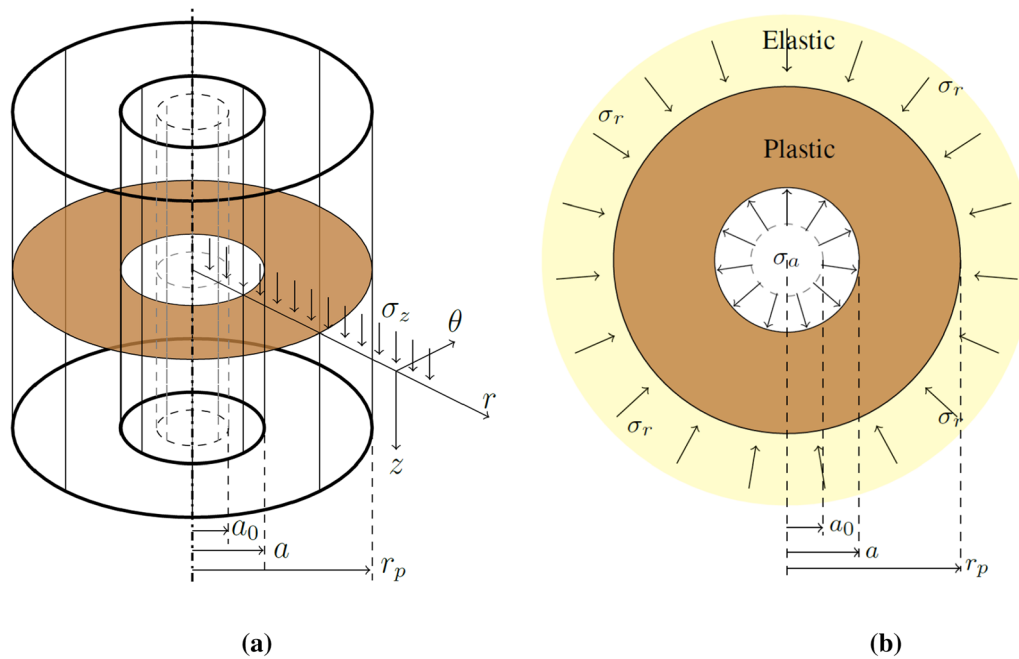
Fig. 1 Geometry of cylindrical cavity expansion: **a** cylindrical cavity; **b** horizontal cross section

where r is the current radial position of a soil particle. As per assumption 3 above, total and effective stresses are the same.

Under drained conditions, the Eulerian equation for a soil particle at a specific moment with the aid of the auxiliary independent variable ξ proposed by Chen and Abousleiman [8] can be converted to the Lagrangian form as

$$\xi = \frac{u_r}{r} = \frac{r - r_0}{r} \qquad (2)$$

2.2 Constitutive model: S-CLAY1S

The S-CLAY1S model, developed by Karstunen et al. [16], is an extension of the S-CLAY1 model [40] incorporating the influence of bonding and destructuration. Anisotropic plastic behaviour is included in the model through an inclined yield surface and a rotational component of hardening to represent the development or erasure of fabric anisotropy during plastic straining. Soil structure is modelled using intrinsic and natural yield surfaces [14]. To make the paper self-contained, the two yield surfaces (intrinsic and natural) and the three hardening laws of the S-CLAY1S model are summarized in the following.

For the simplified conditions of a triaxial stress space and for an initial cross-anisotropy fabric with the main axis being the vertical one (e.g. a vertically cut sample), the yield function can be expressed as [40]

$$f_y = \left(q - \alpha p'\right)^2 - \left(M^2 - \alpha^2\right)\left(p'_m - p'\right)p \qquad (3)$$

where q is the deviatoric stress, p' is the mean effective stress, M is the critical state value of the stress ratio (where $\eta = q/p'$) and p'_m and α define the size and inclination of the natural yield curve, respectively (Fig. 2).

The intrinsic yield surface is of smaller size but same orientation as the yield curve of the natural soil (Fig. 2). The size of the intrinsic yield surface is defined by the state variable p'_{mi} which is linked to the size of the natural yield surface by
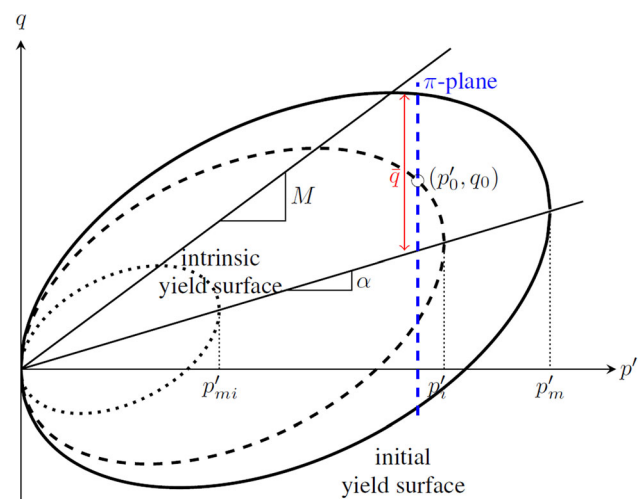
Fig. 2 The S-CLAY1S natural and intrinsic yield surfaces in triaxial stress space and visualization of invariant $\bar{q}$

$$p'_m = (1 + \chi)p'_{mi} \tag{4}$$

where χ defines the amount of bonding.

The first hardening law is analogous to that of the MCC and describes the change of size of the yield curve, which is assumed to be related solely to plastic volumetric strains (as in MCC)

$$\mathrm{d}p'_{mi} = \frac{\upsilon p'_{mi}}{\lambda_i - \kappa}\mathrm{d}\varepsilon^p_v \tag{5}$$

where υ is the specific volume, λ_i is the slope of the intrinsic post-yield compression curve in the $\upsilon - \ln p'$ plane and κ is the slope of the swelling line in the compression plane.

The second hardening law (rotational hardening) describes the change of inclination of the yield curve produced by plastic straining, both volumetric and shear strains.

$$\mathrm{d}\alpha = \omega\left[\left(\frac{3\eta}{4} - \alpha\right)\langle \mathrm{d}\varepsilon^p_v\rangle + \omega_d\left(\frac{\eta}{3} - \alpha\right)|\mathrm{d}\varepsilon^p_d|\right] \tag{6}$$

where ω is a material constant that controls the absolute effectiveness of plastic strains in rotating the yield surface towards the target value. Similarly, ω_d controls the relative effectiveness of shear and volumetric strains.

The third hardening law (destructuration) [16] describes the degradation of bonding with plastic straining by both volumetric and shear strains.

$$\mathrm{d}\chi = -\xi\chi\big(|\mathrm{d}\varepsilon^p_v| + \xi_\mathrm{d}|\mathrm{d}\varepsilon^p_d|\big) \tag{7}$$

where ξ and ξ_d are two additional model constants controlling the rate of degradation (in an analogous manner to ω and ω_d in Eq. 6). Full details of the hardening laws and determination of the model constants may be found in [16, 40].

2.3 Invariants

The natural yield surface of the model (Fig. 2) can be expressed in generalized form as

$$f_y = \frac{3}{2}\big(\boldsymbol{\sigma'_d} - \boldsymbol{\alpha}_d p'\big)^T\big(\boldsymbol{\sigma'_d} - \boldsymbol{\alpha}_d p'\big) - \big(M^2 - \boldsymbol{\alpha}_d^T\boldsymbol{\alpha}_d\big)\big(p'_m - p'\big)p' \tag{8}$$

where

$$\boldsymbol{\sigma'_d} = \big[\, \sigma'_r - p' \quad \sigma'_\theta - p' \quad \sigma'_z - p' \,\big]^T \tag{9}$$

and

$$\boldsymbol{\alpha_d} = \big[\, \alpha_r - 1 \quad \alpha_\theta - 1 \quad \alpha_z - 1 \,\big]^T \tag{10}$$

$$p' = \frac{\big(\sigma'_r + \sigma'_\theta + \sigma'_z\big)}{3}. \tag{11}$$

Sivasithamparam and Castro [34] proposed a new invariant for the S-CLAY1 model ($\overline{q}$), which simplifies the development of mathematical solutions for cylindrical cavity expansion in plastic anisotropic soils. The same invariant was also used for S-CLAY1S [35]

$$\overline{q} = \sqrt{\frac{3}{2}}Q \tag{12}$$

where

$$Q = \big(\boldsymbol{\sigma'_d} - \boldsymbol{\alpha}_d p'\big)^T\big(\boldsymbol{\sigma'_d} - \boldsymbol{\alpha}_d p'\big) = s_r^2 + s_\theta^2 + s_z^2 \tag{13}$$

and s_i are the following deviatoric stresses

$$s_i = \sigma'^d_i - \alpha^d_i p' = \sigma'_i - \big(\alpha^d_i + 1\big)p' \quad \text{for } i = r, \theta, z \tag{14}$$

and α^d_i are deviatoric components of the fabric tensor.

Using this invariant ($\overline{q}$), the natural yield surface of the S-CLAY1S model has a similar form as that of isotropic Cam clay models

$$f_y = \overline{q}^2 - \big(M^2 - \alpha^2\big)\big(p'_m - p'\big)p'. \tag{15}$$

2.4 Elastoplastic stiffness matrix

The increments of elastic strains in r, θ and z directions may be obtained using the isotropic linear elastic stress–strain relationship as

$$\begin{Bmatrix} \mathrm{d}\varepsilon^e_r \\ \mathrm{d}\varepsilon^e_\theta \\ \mathrm{d}\varepsilon^e_z \end{Bmatrix} = \frac{1}{E}\begin{bmatrix} 1 & -v & -v \\ -v & 1 & -v \\ -v & -v & 1 \end{bmatrix} \cdot \begin{Bmatrix} \mathrm{d}\sigma'_r \\ \mathrm{d}\sigma'_\theta \\ \mathrm{d}\sigma'_z \end{Bmatrix} \tag{16}$$

where Young's modulus E is defined in terms of shear modulus G and Poisson's ratio v as

$$E = G(1 + v). \tag{17}$$

G is calculated in the S-CLAY1S model using the current stress state as

$$G = \frac{3(1 - 2v)\upsilon}{2(1 + v)\kappa}p' \tag{18}$$

The components of plastic strain increments $\mathrm{d}\boldsymbol{\varepsilon}^p$ in r, θ and z directions are calculated using the plastic multiplier Λ for the S-CLAY1S model, which considers an associated flow rule.

$$\begin{Bmatrix} \mathrm{d}\varepsilon^p_r \\ \mathrm{d}\varepsilon^p_\theta \\ \mathrm{d}\varepsilon^p_z \end{Bmatrix} = \Lambda \cdot \begin{Bmatrix} \dfrac{\partial f_y}{\partial \sigma'_r} \\[4pt] \dfrac{\partial f_y}{\partial \sigma'_\theta} \\[4pt] \dfrac{\partial f_y}{\partial \sigma'_z} \end{Bmatrix} \tag{19}$$

The plastic multiplier can be written in a matrix form as

$$\Lambda = \mathcal{H} \begin{bmatrix} \dfrac{\partial f_y}{\partial \sigma'_r} & \dfrac{\partial f_y}{\partial \sigma'_\theta} & \dfrac{\partial f_y}{\partial \sigma'_z} \end{bmatrix} \begin{Bmatrix} d\sigma'_r \\ d\sigma'_\theta \\ d\sigma'_z \end{Bmatrix} \tag{20}$$

where

$$\mathcal{H} = -\frac{1}{\mathcal{H}_0 + \mathcal{H}_\alpha + \mathcal{H}_\chi} \tag{21}$$

$$\mathcal{H}_0 = \frac{\partial f_y}{\partial p'_{mi}} \frac{\partial p'_{mi}}{\partial \varepsilon^p_v} \frac{\partial f_y}{\partial p'} \tag{22}$$

$$\mathcal{H}_\alpha = \left\{ \frac{\partial f_y}{\partial \boldsymbol{\alpha}^d} \right\}^T$$
$$\left[\left\{ \frac{\partial \boldsymbol{\alpha}^d}{\partial \varepsilon^p_v} \right\} \cdot \left\langle \frac{\partial f_y}{\partial p'} \right\rangle + \left\{ \frac{\partial \boldsymbol{\alpha}^d}{\partial \varepsilon^p_d} \right\} \cdot \sqrt{\frac{2}{3} \left\{ \frac{\partial f_y}{\partial \boldsymbol{\sigma}'^d} \right\} \cdot \left\{ \frac{\partial f_y}{\partial \boldsymbol{\sigma}'^d} \right\}} \right] \tag{23}$$

$$\mathcal{H}_\chi = \frac{\partial f_y}{\partial \chi} \left[\frac{\partial \chi}{\partial \varepsilon^p_v} \left| \frac{\partial f_y}{\partial p'} \right| + \frac{\partial \chi}{\partial \varepsilon^p_d} \sqrt{\frac{2}{3} \left\{ \frac{\partial f_y}{\partial \boldsymbol{\sigma}'^d} \right\} \cdot \left\{ \frac{\partial f_y}{\partial \boldsymbol{\sigma}'^d} \right\}} \right] \tag{24}$$

All required derivatives and the derivation of the plastic multiplier are presented in Appendixes 1 and 2, respectively.

Using decomposition of the strain vector ($d\boldsymbol{\varepsilon} = d\boldsymbol{\varepsilon}^e + d\boldsymbol{\varepsilon}^p$) and Eqs. (16–24), the elastoplastic constitutive equations in the form of compliance and stiffness matrixes can be derived as

$$\begin{Bmatrix} d\varepsilon_r \\ d\varepsilon_\theta \\ d\varepsilon_z \end{Bmatrix} = \begin{bmatrix} \dfrac{1}{E} + \mathcal{H}n_r^2 & -\dfrac{v}{E} + \mathcal{H}n_r n_\theta & -\dfrac{v}{E} + \mathcal{H}n_r n_z \\ -\dfrac{v}{E} + \mathcal{H}n_\theta n_r & \dfrac{1}{E} + \mathcal{H}n_\theta^2 & -\dfrac{v}{E} + \mathcal{H}n_\theta n_z \\ -\dfrac{v}{E} + \mathcal{H}n_z n_r & -\dfrac{v}{E} + \mathcal{H}n_z n_\theta & \dfrac{1}{E} + \mathcal{H}n_z^2 \end{bmatrix}$$
$$\cdot \begin{Bmatrix} d\sigma'_r \\ d\sigma'_\theta \\ d\sigma'_z \end{Bmatrix} \tag{25}$$

$$\begin{Bmatrix} d\sigma'_r \\ d\sigma'_\theta \\ d\sigma'_z \end{Bmatrix} = \frac{1}{\Gamma} \begin{bmatrix} c_{11} & c_{12} & c_{13} \\ c_{21} & c_{22} & c_{23} \\ c_{31} & c_{32} & c_{33} \end{bmatrix} \cdot \begin{Bmatrix} d\varepsilon_r \\ d\varepsilon_\theta \\ d\varepsilon_z \end{Bmatrix} \tag{26}$$

All terms in Eq. (26) are defined in Appendix 3.

2.5 Rotational hardening rule

As derived by Sivasithamparam and Castro [34], the changes in the fabric components ($d\alpha^d_r$, $d\alpha^d_\theta$ and $d\alpha^d_z$) with the radial direction are

$$\frac{d\alpha^d_i}{dr} = \Phi_i \mathcal{H} \left(n_r \frac{d\sigma'_r}{dr} + n_\theta \frac{d\sigma'_\theta}{dr} + n_z \frac{d\sigma'_z}{dr} \right) \quad \text{for } i = r, \theta, z \tag{27}$$

where

$$\Phi_i = \omega \left(\left(\frac{3(\sigma'_i - p')}{4p'} - \alpha^d_i \right) \left\langle \frac{\partial f_y}{\partial p'} \right\rangle \right.$$
$$\left. + \omega_d \left(\frac{(\sigma'_i - p')}{3p'} - \alpha^d_i \right) \sqrt{\frac{2}{3} \left\{ \frac{\partial f_y}{\partial \boldsymbol{\sigma}'^d} \right\} \cdot \left\{ \frac{\partial f_y}{\partial \boldsymbol{\sigma}'^d} \right\}} \right) \tag{28}$$
$$\text{for } i = r, \theta, z$$

2.6 Bonding and destructuration

The degradation of bonding with plastic straining is given by the destructuration hardening law (Eq. 7). In three dimensions, the plastic strain increments $d\varepsilon^p_v$ and $d\varepsilon^p_d$ are defined as

$$d\varepsilon^p_v = \Lambda \frac{\partial f_y}{\partial p'} \tag{29}$$

$$d\varepsilon^p_d = \Lambda \sqrt{\frac{2}{3} \left\{ \frac{\partial f_y}{\partial \boldsymbol{\sigma}'^d} \right\} \cdot \left\{ \frac{\partial f_y}{\partial \boldsymbol{\sigma}'^d} \right\}} \tag{30}$$

Degradation of bonding along the radial direction can be obtained by substituting Eqs. (29–30) with Eq. (20) (plastic multiplier) into Eq. (7).

$$\frac{d\chi}{dr} = \Omega \mathcal{H} \left(n_r \frac{d\sigma'_r}{dr} + n_\theta \frac{d\sigma'_\theta}{dr} + n_z \frac{d\sigma'_z}{dr} \right) \tag{31}$$

where

$$\Omega = \chi \xi \left(\left\langle \frac{\partial f_y}{\partial p'} \right\rangle + \xi_d \sqrt{\frac{2}{3} \left\{ \frac{\partial f_y}{\partial \boldsymbol{\sigma}'^d} \right\} \cdot \left\{ \frac{\partial f_y}{\partial \boldsymbol{\sigma}'^d} \right\}} \right) \tag{32}$$

2.7 Hardening rule of the intrinsic yield surface

The changes in size of the intrinsic yield surface are provided by the hardening law (Eq. 5) and can be obtained as

$$dp'_{mi} = \Lambda \frac{\upsilon}{\lambda_i - \kappa} p'_{mi} \frac{\partial f_y}{\partial p'_i} \tag{33}$$

2.8 Solution procedure

The radial and tangential strain increments may be defined in natural strain form as

$$d\varepsilon_r = -\frac{\partial(dr)}{\partial r} \quad \text{and} \quad d\varepsilon_\theta = -\frac{dr}{r} \tag{34}$$

where r and dr are position of a material particle in the radial direction and change in the position of that particle, respectively.

For cylindrical cavity and plane strain conditions, the vertical strain is zero, i.e. $d\varepsilon_z = 0$, and the volumetric strain

$$d\varepsilon_v = d\varepsilon_r + d\varepsilon_\theta \tag{35}$$

The auxiliary independent variable ξ defined in Eq. (2) can be written in differential form as

$$\frac{dr}{r} = \frac{d\xi}{1 - \xi} \tag{36}$$

By substituting Eqs. (34, 36) and $d\varepsilon_v = \frac{dv}{v}$ into Eq. (35)

$$d\varepsilon_r = -\frac{dv}{v} + \frac{d\xi}{1 - \xi} \tag{37}$$

By substituting Eq. (34, 36) into (26, 27, 31), applying plane strain conditions, i.e. $d\varepsilon_z = 0$, and following the approach used by Chen and Abousleiman [8], the change of specific volume can be obtained from Eqs. (2, 34, 37), and the following eight partial differential equations in terms of the auxiliary variable ξ are found (three corresponding to stress increments, one to specific volume change, three to rotation of the yield surface and one to destructuration)

$$\frac{d\sigma'_r}{d\xi} = -\frac{\sigma'_r - \sigma'_\theta}{1 - \xi - \frac{v_0}{v(1-\xi)}}$$

$$\frac{d\sigma'_\theta}{d\xi} = -\frac{c_{12}}{c_{11}}\left[\frac{\sigma'_r - \sigma'_\theta}{1 - \xi - \frac{v_0}{v(1-\xi)}} + \frac{c_{11} - c_{12}}{\Gamma(1-\xi)}\right] - \frac{(c_{22} - c_{12})}{\Gamma(1-\xi)}$$

$$\frac{d\sigma'_z}{d\xi} = -\frac{c_{31}}{c_{11}}\left[\frac{\sigma'_r - \sigma'_\theta}{1 - \xi - \frac{v_0}{v(1-\xi)}} + \frac{c_{11} - c_{12}}{\Gamma(1-\xi)}\right] - \frac{(c_{32} - c_{31})}{\Gamma(1-\xi)}$$

$$\frac{dv}{d\xi} = \frac{\Gamma v}{c_{11}}\left[\frac{\sigma'_r - \sigma'_\theta}{1 - \xi - \frac{v_0}{v(1-\xi)}} + \frac{c_{11} - c_{12}}{\Gamma(1-\xi)}\right]$$

$$\frac{d\alpha_r^d}{d\xi} = \Phi_r\mathcal{H}\left(n_r\frac{d\sigma'_r}{d\xi} + n_\theta\frac{d\sigma'_\theta}{d\xi} + n_z\frac{d\sigma'_z}{d\xi}\right)$$

$$\frac{d\alpha_\theta^d}{d\xi} = \Phi_\theta\mathcal{H}\left(n_r\frac{d\sigma'_r}{d\xi} + n_\theta\frac{d\sigma'_\theta}{d\xi} + n_z\frac{d\sigma'_z}{d\xi}\right)$$

$$\frac{d\alpha_z^d}{d\xi} = \Phi_z\mathcal{H}\left(n_r\frac{d\sigma'_r}{d\xi} + n_\theta\frac{d\sigma'_\theta}{d\xi} + n_z\frac{d\sigma'_z}{d\xi}\right)$$

$$\frac{d\chi}{d\xi} = \Omega\mathcal{H}\left(n_r\frac{d\sigma'_r}{d\xi} + n_\theta\frac{d\sigma'_\theta}{d\xi} + n_z\frac{d\sigma'_z}{d\xi}\right)$$

$$\tag{38}$$

The system of eight first-order ordinary differential equations (Eq. 38) governs the expansion of the cylindrical cavity in the plastic region. Boundary conditions for the elastic/plastic boundary and the elastic solution (Appendix 4) are required for the complete mathematical formulation of the problem. The corresponding stress state at the

elastic/plastic boundary is the same as that for the undrained case of the S-CLAY1S model [35] because the natural yield surface is the same (Fig. 2) and the volumetric strains are null in the elastic region (Appendix 4). Thus, the specific volume and the stresses at the elastic/plastic interface are

$$v_p = v_0 \tag{39}$$

$$\sigma'_{z,p} = \frac{3}{1 + 2K_0}p'_0$$

$$\sigma'_{r,p} = \sigma'_{r0} + \sqrt{\frac{1}{3}\left(q^2 - (\sigma'_{z0} - K_0\sigma'_{z0})^2\right)} \tag{40}$$

$$\sigma'_{\theta,p} = \sigma'_{\theta0} - \sqrt{\frac{1}{3}\left(q^2 - (\sigma'_{z0} - K_0\sigma'_{z0})^2\right)}$$

where

$$\sigma'_{r0} = \sigma'_{\theta0} = \frac{3K_0}{1 + 2K_0}p'_0 \quad \text{and} \quad \sigma'_{z0} = \frac{3}{1 + 2K_0}p'_0 \tag{41}$$

and

$$q = \sqrt{q_0^2 + \left(\overline{q}^2 - (q_0 - \alpha p'_0)^2\right)} \tag{42}$$

$$q_0 = \sqrt{\frac{3}{2}\left((\sigma'_{r0} - p'_0)^2 + (\sigma'_{\theta0} - p'_0)^2 + (\sigma'_{z0} - p'_0)^2\right)} \tag{43}$$

$$\overline{q} = \sqrt{(M^2 - \alpha_0^2)(p'_m - p'_0)p'} \tag{44}$$

Equations (39, 40) and the initial values of the amount of bonding and the fabric tensor (anisotropic components) are the initial conditions for solving the differential equations in Eq. (38). The position of the elastic/plastic interface using the auxiliary variable, ξ_p, is

$$\xi_p = \left(\frac{u_r}{r}\right)_{r=r_p} = \frac{\sigma'_{r,p} - \sigma'_{r0}}{2G_0} \tag{45}$$

As presented by Chen and Abousleiman [8], a relationship between ξ and r can be written in the form of the specific volume

$$\frac{dr}{r} = \frac{v_\xi(1 - \xi)}{v_\xi(1 - \xi)^2 - v_0}d\xi \tag{46}$$

Integrating the above equation, the material position, r, can be expressed as

$$\frac{r}{a} = \exp\left(\int_{\xi_a}^{\xi} \frac{v_\xi(1 - \xi)}{v_\xi(1 - \xi)^2 - v_0}d\xi\right) \tag{47}$$

where ξ_a is the value of the auxiliary variable at the cavity wall and is $\xi_a = 1 - \left(\frac{a}{a_0}\right)$.

Substituting Eq. (45) into (47), the position of the elastic/plastic boundary may be obtained

$$\frac{r_p}{a} = \exp\left(\int_{\xi_a}^{\xi_p} \frac{\upsilon_\xi(1-\xi)}{\upsilon_\xi(1-\xi)^2 - \upsilon_0} \mathrm{d}\xi\right)$$ (48)

The system of equations (Eq. 38), imposing the boundary conditions at the elastic/plastic interface can be

1.	**Data**: initial stress state, model parameters and a/a_0
2.	Set initial anisotropic components (α_r, α_θ and α_z)
3.	Set initial bonding ($\chi = \chi_0$)
4.	Set initial specific volume ($\upsilon = \upsilon_0$)
5.	Determine stresses at initial yield ($\sigma'_{z,\xi_p}, \sigma'_{r,\xi_p}$ and σ'_{θ,ξ_p})
6.	Set initial $r_x/a = 1$
7.	Transform a/a_0 to auxiliary variable ξ_a

8. **While** ($i \le nstep$)

Solve ξ for given $\xi_a, \xi, \sigma'_{z,\xi_p}, \sigma'_{r,\xi_p}, \sigma'_{\theta,\xi_p}$ and G_0

Solve partial differential equation:

$Y(\sigma, \upsilon, \alpha, \chi) = $lsode($"ODE"$ ($\sigma'_{z,\xi_p}, \sigma'_{r,\xi_p}, \sigma'_{\theta,\xi_p}, \upsilon, \alpha_r^d, \alpha_\theta^d, \alpha_z^d, \chi$), $\{\xi\}$)

lsode:

9. **function** $ydot = ODE$ ($Y, \{\xi\}$)

9.1. Obtain:

$[\sigma'_r \ \sigma'_\theta \ \sigma'_z \ \upsilon \ \alpha_r \ \alpha_\theta \ \alpha_z \ \chi] = Y$

9.2. Calculate:

α_i^d for $i=r,\theta,z$ and α

p', G, E'

$\frac{\partial f_y}{\partial \sigma_i}$ for $i=r,\theta,z$ and hardening modulus $\mathcal{H}$

$c_{11}, c_{12}, c_{13}, c_{22}, c_{23}, c_{33}$ and Γ

Φ_i for $i=r,\theta,z$

Ω degradation of bonding

9.3. Compute:

$d\sigma'_r/d\xi, \ d\sigma'_\theta/d\xi$ and $d\sigma'_z/d\xi$

$d\alpha_r^d/d\xi, \ d\alpha_\theta^d/d\xi$ and $d\alpha_z^d/d\xi$

$\frac{d\upsilon}{d\xi}$ and $\frac{d\chi}{d\xi}$

endfunction

10. Update $r_x/a \leftarrow r_x/a + \Delta r/a$ ($\Delta r/a = (r_p/a - 1)/nstep$)

$i \leftarrow i + 1$

Transform r_x/a to auxiliary variable ξ

11. Get $\sigma'_r, \sigma'_\theta, \sigma'_z, \upsilon, \alpha_r, \alpha_\theta, \alpha_z$ and χ from $Y(\sigma, \upsilon, \alpha, \chi)$

End

12. Calculate excess pore pressure Δu

13. **If** (OCR > 1) Calculate elastic stresses

End

Fig. 3 Solution procedure for solving ordinary differential equations of cylindrical cavity expansion in GNU Octave

solved numerically; here, the standard differential solver 'lsode' available in GNU Octave v4.0 was used. Figure 3 summarizes the solution procedure.

3 Results and discussion

3.1 Validation

Validation of the proposed semi-analytical solution has been performed by comparison of its results with finite element simulations using the commercial code Plaxis 2D 2019 [2]. The S-CLAY1S model has been implemented as a user-defined soil model in Plaxis, using an automatic substepping in combination with a modified Newton–Raphson integration scheme [32, 33].

The geometrical model (Fig. 4) is based on that used by González et al. [15] for plane strain cylindrical cavity expansion. The boundary condition at the outer boundary is a fixed radial stress (equal to the initial value) and free radial displacements. Sensitivity analyses of mesh refinement and load step size were performed to confirm their small influence.

To account for large displacements, the numerical code uses an updated Lagrangian formulation [23] and adopts the co-rotational rate of Kirchhoff stress (also known as Hill stress rate). The details of the implementation can be found in Van Langen [37].

For the sake of comparison with previous studies, Boston blue clay (BBC) is considered and its modified Cam clay (MCC) parameters are taken from Chen and Abousleiman [7] and additional anisotropic parameters from [34] (S-CLAY1) (see Table 2). Additional parameters for intrinsic compressibility, bonding and destructuration are those used in Sivasithamparam and Castro [35], which were based on information available in the literature. These parameters are just for illustrative purposes, without aiming to reach a detailed calibration of the parameters using experimental tests.

BBC is a moderately sensitive marine clay and, for example, Whittle et al. [41] use a value of $S_t = 4.5$. For the S-CLAY1S model, that implies $\chi_0 = 3.5$ (Table 2). For parametric analyses, four times this value ($\chi_0 = 14$) and a null value ($\chi_0 = 0$) have also been used.

The overconsolidation ratio (OCR) of BBC varies with depth. To provide a broad representation of different depths, several OCR values are considered, namely 1, 1.5, 3 and 5. Their corresponding initial state parameters are shown in Table 3 and are the same as in Sivasithamparam and Castro [34, 35] for the sake of comparison.

The results of the finite element simulations perfectly match those of the proposed semi-analytical solution as may be observed in Fig. 5 for the void ratio and stresses

around the cavity as an example. In this paper, the stresses are normalized by the initial vertical stress, either effective or total stress since they are the same. The finite element analyses are slightly less computationally demanding and in slightly better agreement with the semi-analytical solution than for the undrained case [35] because the soil is not incompressible.

3.2 Internal cavity pressure

To expand the cavity, an internal pressure (radial stress), σ_a, must be applied. Its value must monotonically increase to continue with the expansion of the cavity. When the cavity has been notably expanded (around $a/a_0 > 2$), σ_a approaches an asymptotic limit value, sometimes called pressuremeter limit pressure.

Figure 6 shows its variation with the normalized cavity radius for different OCR and χ_0 values. As expected, the radial stress increases with the OCR and decreases with the initial amount of bonding (χ_0). As happens for undrained conditions [35], mechanical overconsolidation and initial bonding have similar effects on the load–displacement curve (Fig. 6), but the influence of the initial bonding is limited beyond values around $\chi_0 > 3.5$. For drained conditions, the radial stress is larger and increases more gradually than for undrained conditions. For example, for $a/a_0 = 2$, the radial stress is around 90% the limit pressure for drained conditions, while it is around 97% for undrained conditions [35].

3.3 Stresses around the cavity

Figure 7 shows the stresses and the specific volume around the cavity when the cavity radius is twice the initial one ($a/a_0 = 2$). For the sake of comparison, results for the case without destructuration (S-CLAY1, i.e. $\lambda = 0.15$ and $\chi_0 = 0$) are also included in Fig. 7. The extension of the plastic annulus depends on the OCR. For normally consolidated conditions, all the material points yield just when the cavity expansion begins, but plastic strains are negligible beyond $r > 10a$.

It is worth noting that the extensions of the plastic annuli are slightly different for the cases with and without destructuration. Their values are the same using the auxiliary variable (Eq. 45), but when that value is converted to the radial coordinate (Eq. 48), they are slightly different because the soil compressibilities, i.e. the specific volume variations, are different.

Near the cavity, the vertical stress is usually the intermediate one and it is equal to the average of the other two (plane strain conditions):
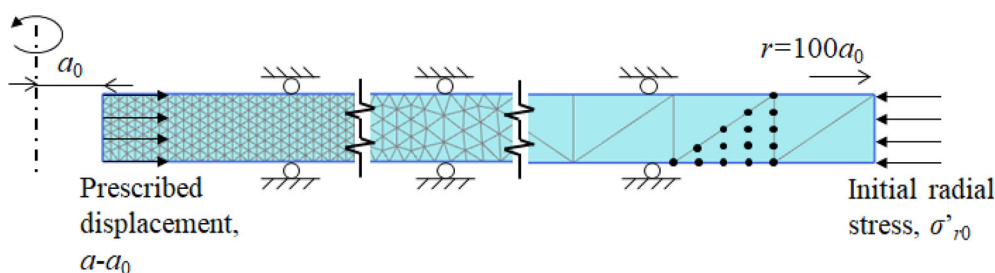
$$\sigma'_z = (\sigma'_r + \sigma'_\theta)/2 \tag{49}$$

Fig. 4 Finite element model for cylindrical cavity expansion

Table 2 Soil properties, Boston blue clay

Basic parameters				Anisotropy*			Destructuration			
κ	v'	λ	M	α_0	ω	ω_d	χ_0	λ_i	ξ	ξ_d
0.03	0.278	0.15	1.2	0.46	80	0.76	3.5	0.12	9	0.2

*Following Wheeler et al. [40]

Table 3 Soil state parameters, Boston blue clay

OCR	σ'_{z0} (kPa)	K_0	e_0	G_0 (kPa)
1	160	0.5	1.09	3873
1.5	160	0.55	1.04	3969
3	120	0.71	1.00	3363
5	100	0.92	0.96	3223
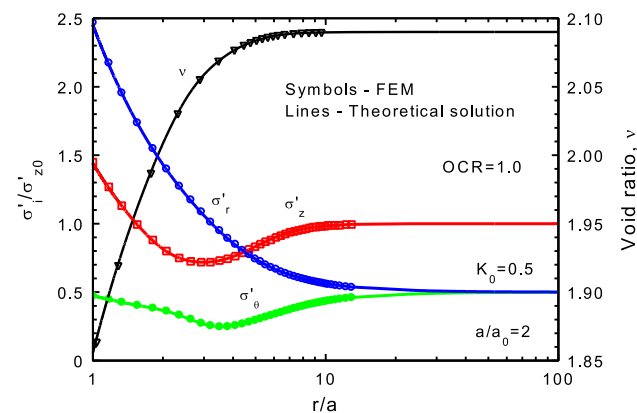
Fig. 5 Validation of the theoretical solution against finite element analyses

When destructuration is considered, critical state (CS) is not usually reached for common expansions of the cavity (e.g. $a/a_0 = 2$) and common rates of destructuration (e.g. $\xi = 9$ and $\xi_d = 0.2$), because very large strains are necessary for a complete loss of structure (fully remoulded state).

(a)

(b)
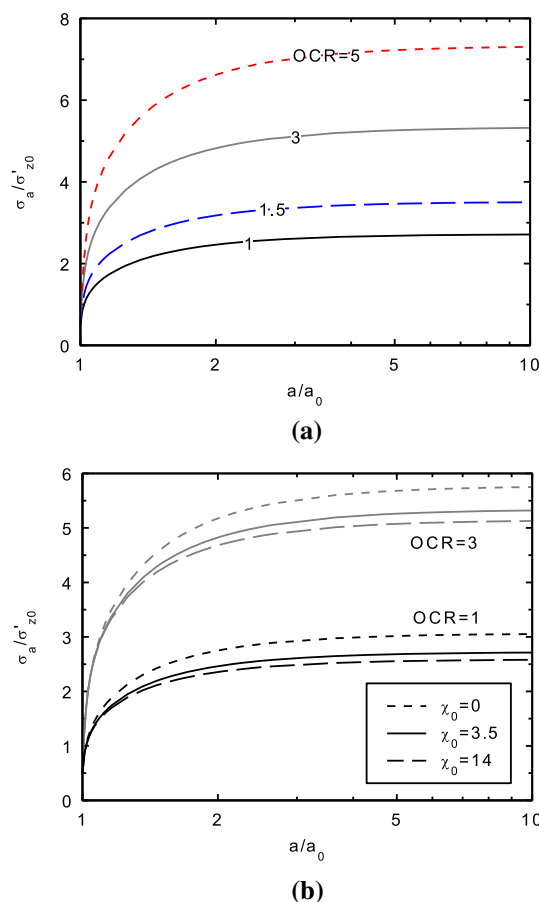
Fig. 6 Radial stress at cavity wall during cavity expansion: **a** influence of overconsolidation; **b** influence of initial bonding
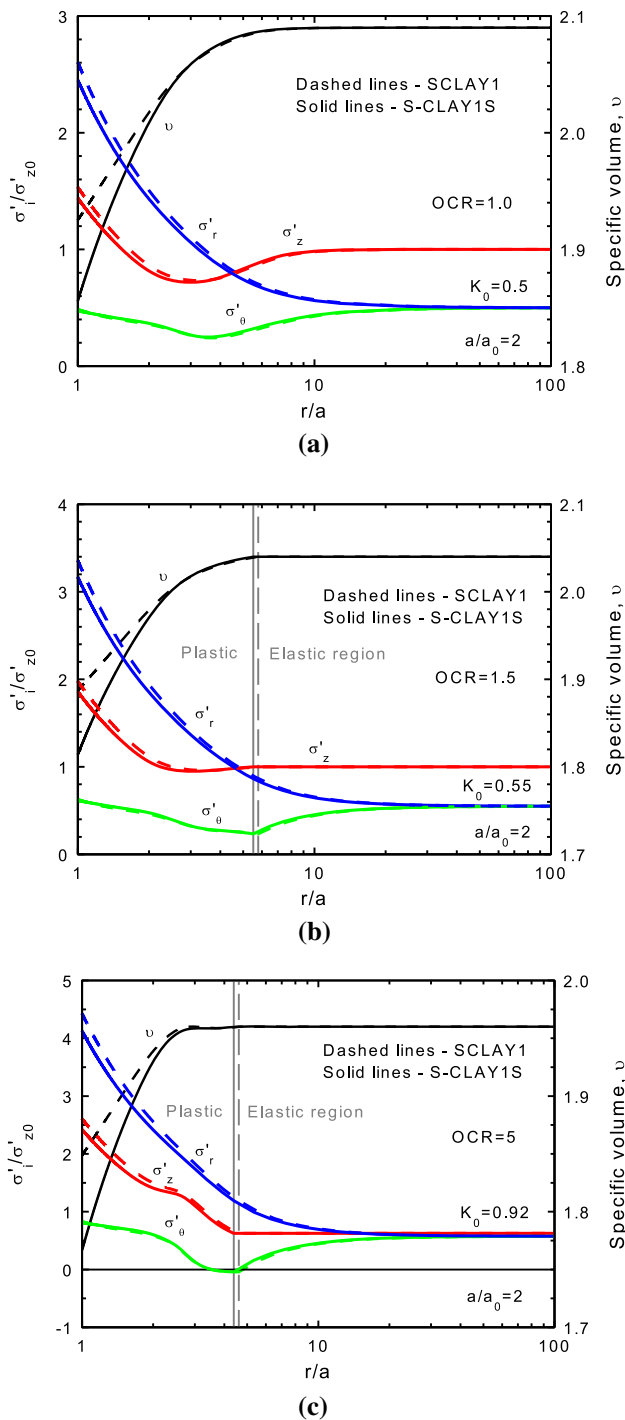
Fig. 7 Influence of destructuration on specific volume and stress distributions around the cavity: **a** OCR = 1; **b** OCR = 1.5; **c** OCR = 5

Normalized effective mean stresses for different OCR values are plotted in Fig. 8. The increase in the effective mean stress may be correlated with the improvement of the soil, e.g. its stiffening. The area of increase in the effective mean stress is limited to 3–4 cavity radii. This area of influence is similar to that of the undrained case [35] and to that measured by some authors (e.g. [1, 26]).
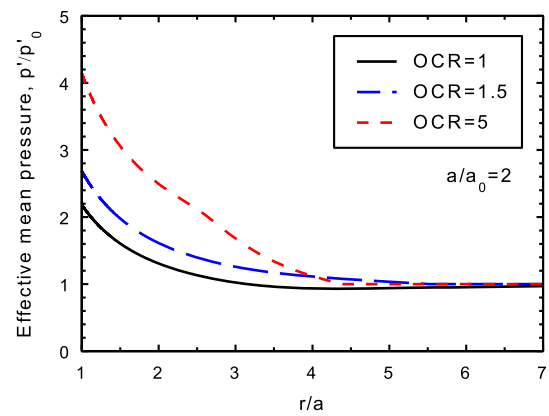
Fig. 8 Increase in effective mean pressure around the cavity

3.4 Specific volume

As well-known, volumetric strains are null in the elastic region (e.g. [43]), but in the plastic region, the soil compresses and the initial void ratio or specific volume decreases (Fig. 7). The loss of bonding near the cavity increases the soil compressibility, and therefore, the specific volume is lower near the cavity when destructuration is considered (S-CLAY1S).

Figure 9 shows the decrease of the specific volume at the cavity wall as the cavity expands for different OCRs and χ_0. When the soil is overconsolidated, the specific volume does not nearly change at the beginning of the cavity expansion, but later, the specific volume reduction is similar to the normally consolidated case. The loss of bonding causes an important reduction of the specific volume from the beginning. The specific volume tends to a final asymptotic value that correspond to CS conditions.

The decrease of the specific volume of a point at the cavity wall during cavity expansion is represented in a $p' - \upsilon$ plane (Fig. 10) for different OCR values, namely 1, 1.5 and 5, and for the cases with and without destructuration, i.e. S-CLAY1S ($\lambda_i = 0.12$ and $\chi_0 = 3.5$) and S-CLAY1 ($\lambda = 0.15$ and $\chi_0 = 0$), respectively. The lines represent the path from the beginning of the expansion (initial specific volume υ_0) ($a/a_0 = 1$) until a cavity expansion large enough to reach the critical state line (CSL), namely $a/a_0 = 10$. It is worth noting that the initial specific volumes for the cases using the S-CLAY1S model are the same ones as those when the S-CLAY1 model is used and those in Sivasithamparam and Castro [35] for the sake of comparison. Consequently, slightly different void ratios of the CSL for different OCRs were obtained when using the S-CLAY1S model. Destructuration causes a further reduction of the specific volume and a slightly lower mean effective stress at CS.
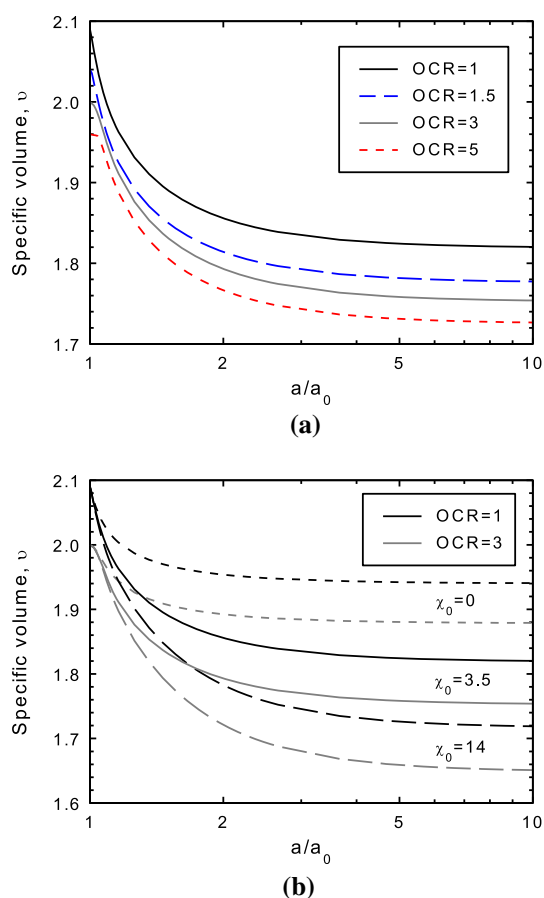
Fig. 9 Specific volume at cavity wall during cavity expansion: **a** influence of overconsolidation; **b** influence of initial bonding
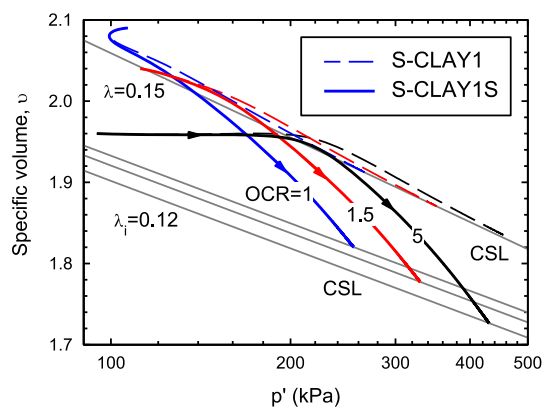
Fig. 10 Specific volume variations with effective mean pressure at cavity wall until $a/a_0 = 10$

3.5 Stress paths

For a better understanding of the problem, it is useful to observe the effective stress paths (ESP) followed by a point at the cavity wall during cavity expansion. Figures 11 and 12 show the stress paths for different OCR values in $p' - q$ stress plane and deviatoric stress plane (π-plane),

respectively. The stress paths illustrate the stress state of a point at the cavity wall from the beginning of the expansion (initial K_0 state) ($a/a_0 = 1$) until a final cavity expansion of $a/a_0 = 10$. In Fig. 11, the point corresponding to $a/a_0 = 2$ is also indicated with an open square symbol for the sake of comparison.

In the $p' - q$ stress plane, if the soil is overconsolidated, the stress paths goes up vertically until reaching the yield surface. It is worth noting that the initial yield surface (YS_0) plotted in Fig. 11 corresponds to the triaxial plane, while yielding is here reached for a different value of the Lode's angle (Fig. 12) [10]. Later, the stress path progressively approaches the CSL. The yield surface rotates towards plain state condition and increases due to the increase in the mean effective pressure caused by the drained expansion of the cavity (Figs. 11 and 12).

The initial amount of bonding (χ_0) does not notably change the followed stress paths (Fig. 13), but higher values of χ_0 cause larger destructurations (Eq. 7), and consequently, lower final stresses.

Figure 12 also shows the path followed by the $\boldsymbol{\alpha} \cdot p'$ vector, which depicts the centre of the anisotropic yield surface. It shows how the yield surface rotates from triaxial compression conditions towards plane strain conditions. Destructuration causes a reduction of effective stresses (p'), but the influence of destructuration on the evolution of fabric anisotropy ($\boldsymbol{\alpha}$) is minor, as it will be presented in the next section.

3.6 Fabric anisotropy

The evolution of fabric anisotropy is quite similar for the cases with and without destructuration, i.e. for the S-CLAY1S and S-CLAY1 models, respectively, (Fig. 14). The anisotropic hardening law (Eq. 6) is the same for both models, and the differences are mainly caused by the differences in the specific volume.

At the cavity wall, the fabric tensor approaches a constant value that may be analytically obtained as

$$\begin{bmatrix} \alpha_r & \alpha_\theta & \alpha_z \end{bmatrix} = \begin{bmatrix} 1 + \sqrt{3}M/9 & 1 - \sqrt{3}M/9 & 1 \end{bmatrix}$$

($\alpha = M/3$), which corresponds to critical state and plane strain conditions (refer to Sivasithamparam and Castro [34] for further details). Please note that this value is the same for both drained and undrained conditions and for the S-CLAY1 and S-CLAY1S models. When destructuration is considered, large strains are necessary to reach CS (i.e., full loss of bonding). For example, in Fig. 14 ($a/a_0 = 2$), α is close to $M/3$, but not exactly $M/3$ yet.
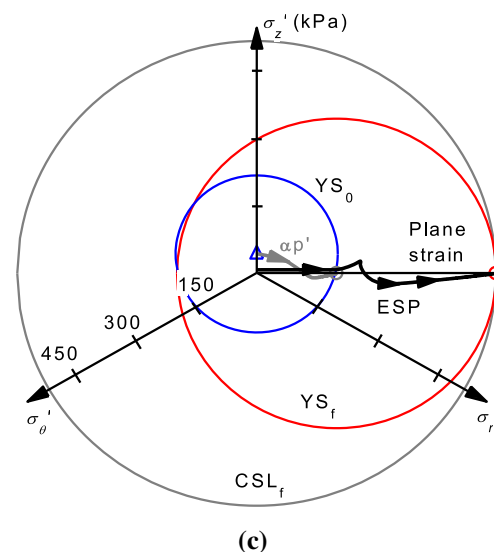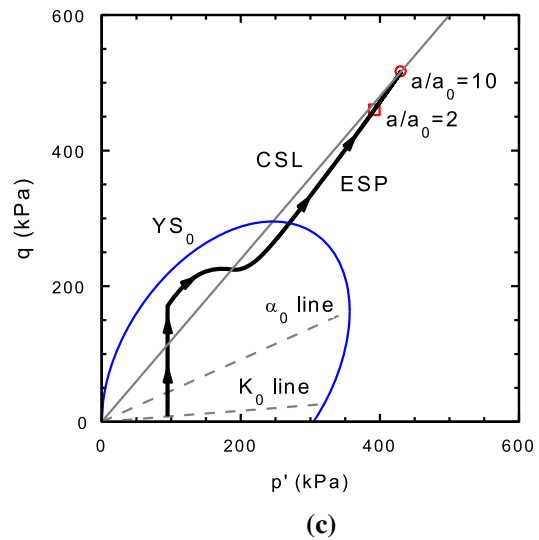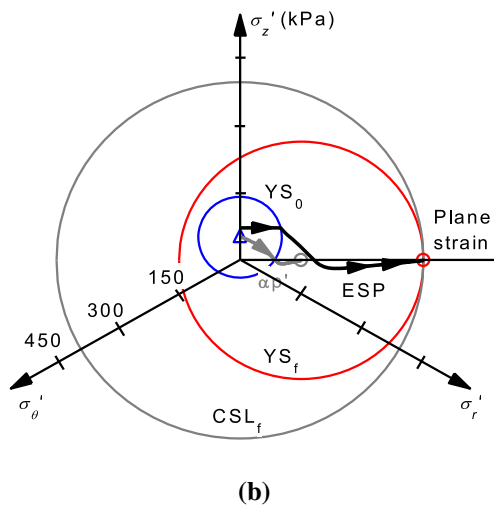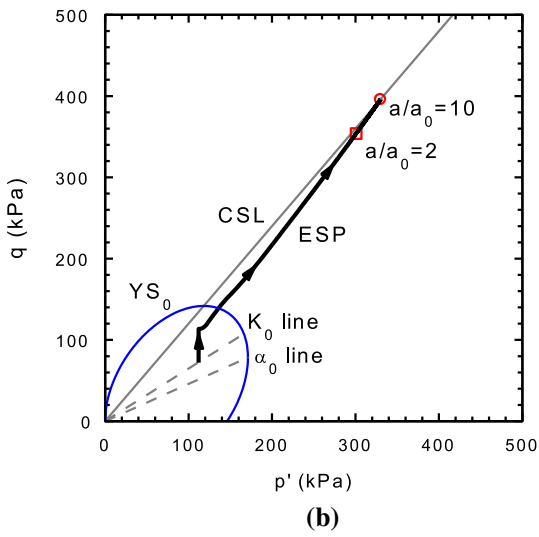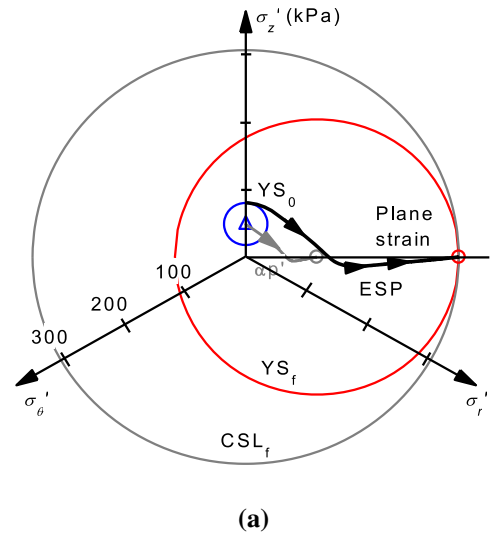
(a)

(b)

(c)
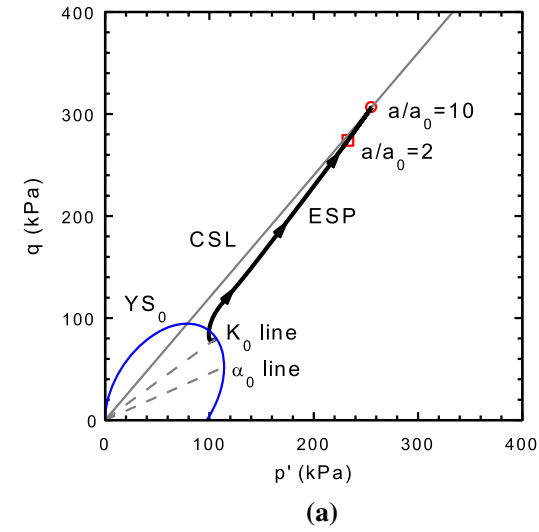
Fig. 11 p'-q stress paths at cavity wall until $a/a_0 = 10$: **a** OCR = 1; **b** OCR = 1.5; **c** OCR = 5

(a)

(b)

(c)

Fig. 12 Stress paths at cavity wall in π-plane until $a/a_0 = 10$: **a** OCR = 1; **b** OCR = 1.5; **c** OCR = 5

3.7 Structure and amount of bonding

Cavity expansion usually generates plastic strains, which in turn cause a loss of bonding of the structured clay (Fig. 15) as per the assumed destructuration hardening law (Eq. 7). The loss of bonding (destructuration) is proportional to the current bonding parameter (Eq. 7). Consequently, the loss of bonding may be normalized by the initial amount of bonding in Fig. 15.

It may be observed in Fig. 15 that the loss of bonding at the cavity wall is nearly independent of OCR, and only the extension of the plastic zone and, consequently, the extension of the zone where the amount of bonding decreases is influenced by OCR. Figure 15 corresponds to the case with $a/a_0 = 2$, but larger radial expansions of the cavity generate larger soil distortions and larger destructuration of the soil, both in terms of extension and amount

(a)

(b)
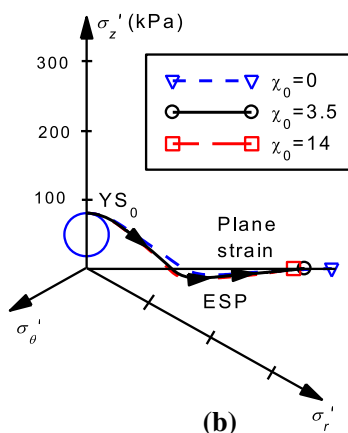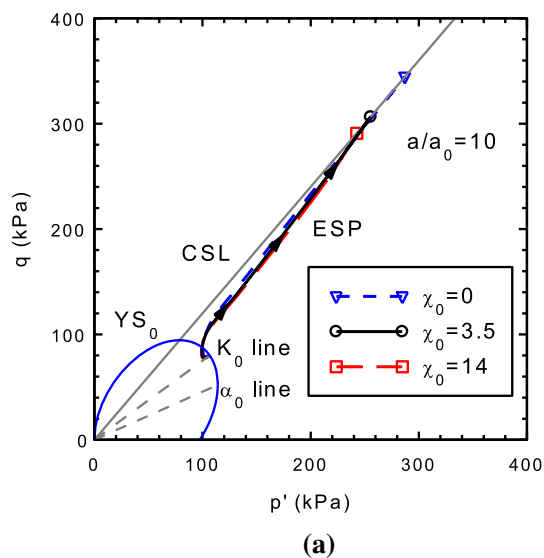
Fig. 13 Influence of initial bonding on stress paths (until $a/a_0 = 10$). **a** p'–q plane; **b** π-plane

(a)

(b)

(c)
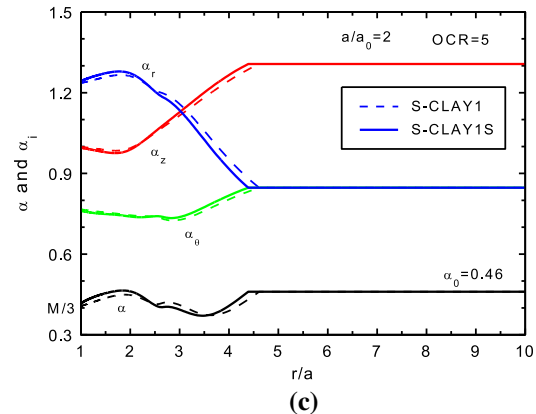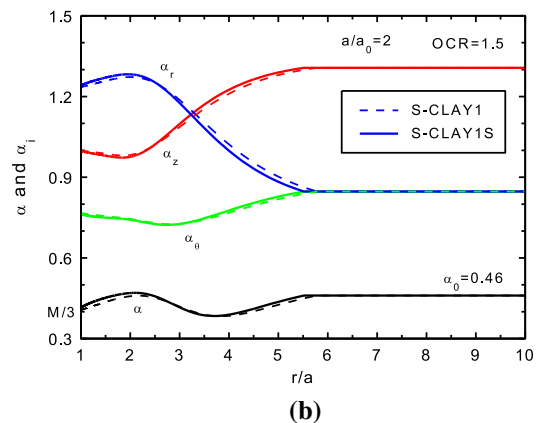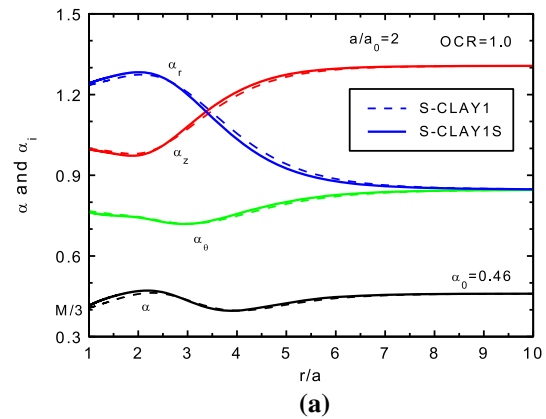
Fig. 14 Changes in fabric anisotropy: **a** OCR = 1; **b** OCR = 1.5; **c** OCR = 5

of destructuration. For example, for $a/a_0 = 10$, full loss of bonding is reached at the cavity wall (Fig. 9).

4 Conclusions

A novel, exact and semi-analytical cylindrical cavity expansion solution for natural clays has been rigorously developed using the S-CLAY1S constitutive model, which
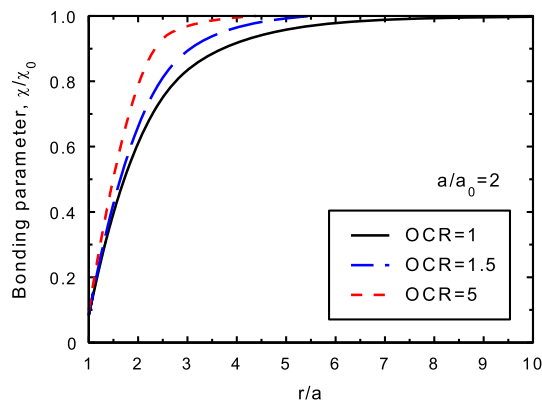
Fig. 15 Loss of bonding caused by cavity expansion

is a Cam clay type of model that considers fabric anisotropy that evolves with plastic strains, structure and gradual degradation of bonding (destructuration) due to plastic straining. The solution involves the numerical integration of a system of eight first-order ordinary differential equations, three of them corresponding to the effective stresses in cylindrical coordinates, other three corresponding to the components of the fabric tensor and one corresponding to the amount of bonding and another for the specific volume.

The semi-analytical solution has been developed using the auxiliary variable introduced by Chen and Abouisleiman 8, and the solution has been validated against finite element analyses, using Boston blue clay as the reference natural clay.

When destructuration is considered, i.e. using the S-CLAY1S model, the solution provides lower values of the effective radial and mean stresses near the cavity wall than those obtained when destructuration is not considered (S-CLAY1). Besides, the specific volume is further reduced due to loss of bonding.

Evolution of fabric anisotropy is similar with both S-CLAY1 and S-CLAY1S soil models. The slight differences are caused by the different soil compressibilities. The initial vertical cross-anisotropy caused by the soil deposition changes towards a radial anisotropy after cavity expansion. Analytical values are provided for the fabric anisotropy at the cavity wall for large cavity expansions, i.e. at CS. Those analytical values are the same for drained and undrained conditions and for both S-CLAY1 and S-CLAY1S soil models.

For common values, the soil near the cavity does not reach CS, i.e. full remoulding and a constant stress state. The loss of bonding extends along the plastic annulus surrounding the cavity (larger for larger OCR and imposed radial displacements), being the largest at the cavity wall and progressively decreasing until a null loss of bonding in the elastic zone.

Appendix 1: Derivatives

The partial derivatives used in the analytical solution are

$$\frac{\partial f_y}{\partial \sigma_i'} = \frac{p'(M^2 - \alpha^2 - \overline{\eta}^2)}{3} + \left(3s_i - s_r\alpha_r^d - s_\theta\alpha_\theta^d - s_z\alpha_z^d\right)$$
for $i = r, \theta, z$

where

$$\overline{\eta} = \frac{\overline{q}}{p'}$$

$$\overline{q} = \sqrt{\frac{3}{2}}Q$$

and

$$\frac{\partial f_y}{\partial p_{mi}'} = -p'(M^2 - \alpha^2)(1 + \chi)$$

$$\frac{\partial p_{mi}'}{\partial \varepsilon_v^p} = \frac{\upsilon p'}{(\lambda_i - \kappa)(1 + \chi)(M^2 - \alpha^2)}\left(M^2 - \alpha^2 + \overline{\eta}^2\right)$$

$$\frac{\partial f_y}{\partial p'} = p'(M^2 - \alpha^2 - \overline{\eta}^2) - 3\left(s_r\alpha_r^d + s_\theta\alpha_\theta^d + s_z\alpha_z^d\right)$$

$$\frac{\partial f_y}{\partial \alpha_i^d} = -3s_i p' + 3\alpha_i^d \frac{\overline{q}^2}{M^2 - \alpha^2} \quad \text{for} \quad i = r, \theta, z$$

$$\frac{\partial f_y}{\partial \sigma_i'^d} = 3s_i \quad \text{for} \quad i = r, \theta, z$$

$$\frac{\partial \alpha_i^d}{\partial \varepsilon_v^p} = \omega\left(\frac{3(\sigma_i' - p')}{4p'} - \alpha_i^d\right) \quad \text{for} \quad i = r, \theta, z$$

$$\frac{\partial \alpha_i^d}{\partial \varepsilon_d^p} = \omega\omega_d\left(\frac{(\sigma_i' - p')}{3p'} - \alpha_i^d\right) \quad \text{for} \quad i = r, \theta, z$$

$$\sqrt{\frac{2}{3}\left\{\frac{\partial f_y}{\partial \boldsymbol{\sigma}'^d}\right\} \cdot \left\{\frac{\partial f_y}{\partial \boldsymbol{\sigma}'^d}\right\}} = 2\overline{q}$$

$$\frac{\partial f_y}{\partial \boldsymbol{\chi}} = -\frac{p'^2}{(1 + \chi)}\left[M^2 - \alpha^2 + \overline{\eta}^2\right]$$

$$\frac{\partial \chi}{\partial \varepsilon_v^p} = -\xi\chi$$

$$\frac{\partial \chi}{\partial \varepsilon_d^p} = -\xi\xi_d\chi$$

Appendix 2: Derivation of the plastic multiplier

The consistency condition ($\dot{f_y} = 0$) is developed as:

$$\dot{f_y} = \frac{\partial f_y}{\partial \sigma'_i} d\sigma'_i + \frac{\partial f_y}{\partial p'_{mi}} dp'_{mi} + \frac{\partial f_y}{\partial \boldsymbol{\alpha_d}} d\boldsymbol{\alpha_d} + \frac{\partial f_y}{\partial \chi} d\chi = 0$$
$$\text{for } i = r, \theta, z$$

and in terms of plastic strains, it is:

$$\dot{f_y} = \frac{\partial f_y}{\partial \sigma'_i} d\sigma'_i + \frac{\partial f_y}{\partial p'_m} \frac{\partial p'_m}{\partial \varepsilon^p_v} d\varepsilon^p_v + \frac{\partial f_y}{\partial \boldsymbol{\alpha_d}} \frac{\partial \boldsymbol{\alpha_d}}{\partial \varepsilon^p_v} d\varepsilon^p_v + \frac{\partial f_y}{\partial \boldsymbol{\alpha_d}} \frac{\partial \boldsymbol{\alpha_d}}{\partial \varepsilon^p_d} \left| d\varepsilon^p_d \right|$$
$$+ \frac{\partial f_y}{\partial \chi} \frac{\partial \chi}{\partial \varepsilon^p_v} d\varepsilon^p_v + \frac{\partial f_y}{\partial \chi} \frac{\partial \chi}{\partial \varepsilon^p_d} \left| d\varepsilon^p_d \right| = 0 \quad \text{for } i = r, \theta, z$$

Thus, the plastic multiplier is

$$\Lambda = -\frac{\frac{\partial f_y}{\partial \sigma'_i} d\sigma'_i}{\frac{\partial f_y}{\partial p'_{mi}} \frac{\partial p'_{mi}}{\partial \varepsilon^p_v} \frac{\partial f_y}{\partial p'} + \left\{ \frac{\partial f_y}{\partial \boldsymbol{\alpha_d}} \right\}^T \left[\left\{ \frac{\partial \boldsymbol{\alpha_d}}{\partial \varepsilon^p_v} \right\} \cdot \frac{\partial f_y}{\partial p'} + \left\{ \frac{\partial \boldsymbol{\alpha_d}}{\partial \varepsilon^p_d} \right\} \cdot \sqrt{\frac{2}{3} \left\{ \frac{\partial f_y}{\partial \boldsymbol{\sigma_d}} \right\} \cdot \left\{ \frac{\partial f_y}{\partial \boldsymbol{\sigma_d}} \right\}} \right] + \frac{\partial f_y}{\partial \chi} \left[\frac{\partial \chi}{\partial \varepsilon^p_v} \left| \frac{\partial f_y}{\partial p'} \right| + \frac{\partial \chi}{\partial \varepsilon^p_d} \sqrt{\frac{2}{3} \left\{ \frac{\partial f_y}{\partial \boldsymbol{\sigma'd}} \right\} \cdot \left\{ \frac{\partial f_y}{\partial \boldsymbol{\sigma'd}} \right\}} \right]}$$

Appendix 3: Elastoplastic solution

$$c_{11} = \frac{1}{E^2} \left(1 - v^2 + E\mathcal{H}n_\theta^2 + 2Ev\mathcal{H}n_\theta n_z + E\mathcal{H}n_z^2 \right)$$

$$c_{12} = c_{21} = \frac{1}{E^2} \left[-E\mathcal{H}(n_\theta + v n_z) + v\left(1 + v - E\mathcal{H}n_\theta n_z + E\mathcal{H}n_z^2 \right) \right]$$

$$c_{13} = c_{31} = \frac{1}{E^2} \left[-E\mathcal{H}n_r(v n_\theta + n_z) + v\left(1 + v - E\mathcal{H}n_\theta^2 + E\mathcal{H}n_\theta n_z \right) \right]$$

$$c_{22} = \frac{1}{E^2} \left(1 - v^2 + E\mathcal{H}n_r^2 + 2Ev\mathcal{H}n_r n_z + E\mathcal{H}n_z^2 \right)$$

$$c_{23} = c_{32} = \frac{1}{E^2} \left[v + v^2 + E\mathcal{H}v n_r^2 - E\mathcal{H}n_\theta n_z - E\mathcal{H}v n_r(n_\theta + n_z) \right]$$

$$c_{33} = \frac{1}{E^2} \left(1 - v^2 + E\mathcal{H}n_r^2 + 2Ev\mathcal{H}n_r n_\theta + E\mathcal{H}n_\theta^2 \right)$$

$$\Gamma = -\frac{1+v}{E^3}$$
$$\begin{bmatrix} (-1 + v + 2v^2) + EH(-1+v)n_r^2 + EH(-1+v)n_\theta^2 \\ -2EHvn_\theta n_z - EHn_z^2 + EHvn_z^2 - 2EHvn_r(n_\theta + n_z) \end{bmatrix}$$

where

$$n_i = \frac{\partial f_y}{\partial \sigma'_i} \quad \text{for } i = r, \theta, z$$

Appendix 4: Elastic solution

The solution for the elastic stresses (σ'_r, σ'_θ, σ'_z) (total and effective stresses are the same here) and the radial displacement (u_r) may be found, for example, in Yu [43]

$$\sigma'_r = \sigma'_H + \left(\sigma'_{r,p} - \sigma'_H \right) \left(\frac{r_p}{r} \right)^2 \tag{50}$$

$$\sigma'_\theta = \sigma'_H + \left(\sigma'_{r,p} - \sigma'_H \right) \left(\frac{r_p}{r} \right)^2 \tag{51}$$

$$\sigma'_z = \sigma'_V \tag{52}$$

$$u_r = \frac{\sigma'_{r,p} - \sigma'_H}{2G_0} \frac{r_p^2}{r} \tag{53}$$

where $\sigma'_{r,p}$ is the radial stress at the elastic/plastic boundary (Eq. 40) and σ'_H and σ'_V are the horizontal and vertical stresses, respectively.

References

1. Bond AJ, Jardine RJ (1991) Effects of installing displacements piles in a high OCR clay. Geotechnique 41(3):341–363
2. Brinkgreve RBJ, Kumarswamy S, Swolfs WM, Zampich L, Ragi Manoj N (2019) Plaxis 2D 2019 Manual. Plaxis bv, Delft
3. Callisto L, Rampello S (2004) An interpretation of structural degradation for three natural clays. Can Geotech J 41:392–407
4. Castro J, Sivasithamparam N (2017) A constitutive model for soft clays incorporating elastic and plastic cross-anisotropy. Materials 10(6):584
5. Chen H, Li L, Li J, Wang H (2019) Stress transform method to undrained and drained expansion of a cylindrical cavity in anisotropic modified cam-clay soils. Comput Geotech 106:128–142
6. Chen H, Li L, Li J, Sun D (2020) Elastoplastic solution to drained expansion of a cylindrical cavity in anisotropic critical-state soils. J Eng Mech 146:04020036
7. Chen SL, Abousleiman YN (2012) Exact undrained elasto-plastic solution for cylindrical cavity expansion in modified Cam Clay soil. Géotechnique 62:447–456
8. Chen SL, Abousleiman YN (2013) Exact drained solution for cylindrical cavity expansion in modified Cam Clay soil. Géotechnique 63:510–517
9. Chen SL, Liu K (2019) Undrained cylindrical cavity expansion in anisotropic critical state soils. Géotechnique 69:189–202
10. Chen SL, Liu K, Castro J, Sivasithamparam N (2019) Discussion of undrained cylindrical cavity expansion in anisotropic critical state soils. Géotechnique 69:1026–1028

11. Dafalias YF (1986) An anisotropic critical state soil plasticity model. Mech Res Commun 13:341–347

12. Dafalias YF (1987) An anisotropic critical state clay plasticity model. In: Desai CS, Krempl E, Kiousis PD, Kundu T (eds) Proceedings of the constitutive laws for engineering materials: theory and applications, Tucson, AZ, USA. Elsevier, New York, NY, USA, pp 513–521

13. Deotti LOG, Karstunen M, Almeida MCF, Almeida MS (2017) Modeling of laboratory tests on Saint-Roch-de-l'Achigan clay with S-CLAY1S model. Int J Geomech 17:06016018

14. Gens A, Nova R (1993) Conceptual bases for a constitutive model for bonded soils and weak rocks. In: Proceedings of an international symposium on hard soils–soft rocks, Athens, Greece, pp 485–494

15. González N, Arroyo M, Gens A (2009) Identification of bonded clay parameters in SBPM tests: a numerical study. Soils Found 49:329–340

16. Karstunen M, Krenn H, Wheeler SJ, Koskinen M, Zentar R (2005) Effect of anisotropy and destructuration on the behaviour of Murro test embankment. Int J Geomech 5:87–97

17. Ladd CC, Germaine JT, Baligh MM, Lacasse SM (1980) Evaluation of self-boring pressuremeter tests in Boston blue clay. Federal Highway Administration, Report n° FHWA/RD-80/052. Nat. Tech. Info. Service, Springfield, Virginia, USA

18. Li C, Zou J-F, Zhou H (2019) Cavity expansion in k0 consolidated clay. Eur J Enviro Civil Eng. https://doi.org/10.1080/19648189.2019.1605937

19. Li J, Gong W, Li L, Liu F (2017) Drained elastoplastic solution for cylindrical cavity expansion in K_0-consolidated anisotropic soil. J Eng Mech 143:04017133

20. Li L, Li J, Sun D (2016) Anisotropically elasto-plastic solution to undrained cylindrical cavity expansion in K_0-consolidated clay. Comput Geotech 73:83–90

21. Liu K, Chen SL (2019) Analysis of cylindrical cavity expansion in anisotropic critical state soils under drained conditions. Can Geotech J 56:675–686

22. Liu K, Chen SL, Voyiadjis GZ (2019) Integration of anisotropic modified Cam Clay model in finite element analysis: formulation, validation, and application. Comput Geotech 116:103198

23. McMeeking RM, Rice JR (1975) Finite-element formulation for problems of large elastic-plastic deformation. Int J Solids Struct 11:601–616

24. Prévost JH, Hoëg K (1975) Analysis of pressuremeter in strain softening soil. J Geotech Eng Div ASCE 101:717–732

25. Randolph MF, Carter JP, Wroth CP (1979) Driven piles in clay-the effects of installation and subsequent consolidation. Géotechnique 29:361–393

26. Roy M, Lemieux M (1986) Long-term behaviour of reconsolidated clay around a driven pile. Can Geotech J 23(1):23–29

27. Rouainia M, Muir Wood D (2000) A kinematic hardening constitutive model for natural clays with loss of structure. Géotechnique 50:153–164

28. Rouainia M, Panayides S, Arroyo M, Gens A (2020) A pressuremeter-based evaluation of structure in London Clay using a kinematic hardening constitutive model. Acta Geotech 15:2089–2210

29. Semnani SJ, White JA, Borja RI (2016) Thermoplasticity and strain localization in transversely isotropic materials based on anisotropic critical state plasticity. Int J Num Anal Methods Geomech 40:2423–2449

30. Silvestri V (2003) Assessment of self-boring pressuremeter tests in sensitive clay. Can Geotech J 40:362–387

31. Silvestri V, Tabib C (2018) Application of cylindrical cavity expansion in MCC model to a sensitive clay under K_0 consolidation. J Mater Civ Eng 30:04018155

32. Sivasithamparam N (2012) Development and implementation of advanced soft soil models in finite elements. Ph.D. thesis, University of Strathlcyde, Glasgow

33. Sivasithamparam N, Castro J (2016) An anisotropic elastoplastic model for soft clays based on logarithmic contractancy. Int J Num Anal Methods Geomech 40:596–621

34. Sivasithamparam N, Castro J (2018) Undrained expansion of a cylindrical cavity in clays with fabric anisotropy: theoretical solution. Acta Geotech 13:729–746

35. Sivasithamparam N, Castro J (2020) Undrained cylindrical cavity expansion in clays with fabric anisotropy and structure: theoretical solution. Comput Geotech 120:103386

36. Sun DA, Matsuoka H, Yao YP, Ishii H (2004) An anisotropic hardening elastoplastic model for clays and sands and its application to FE analysis. Comput Geotech 31:37–46

37. Van Langen H (1991) Numerical analysis of soil-structure interaction. Ph.D. thesis, Delft University of Technology, Delft, the Netherlands

38. Vesic AS (1972) Expansion of cavities in infinite soil mass. J Soil Mech Found Div ASCE 98:265–290

39. Vrakas A (2016) A rigorous semi-analytical solution for undrained cylindrical cavity expansion in critical state soils. Int J Num Anal Meth Geomech 40(15):2137–2160

40. Wheeler SJ, Naatanen A, Karstunen M, Lojander M (2003) An anisotropic elastoplastic model for soft clays. Can Geotech J 40(2):403–418

41. Whittle AJ, DeGroot DJ, Ladd CC, Seah T-H (1994) Model prediction of anisotropic behavior of Boston blue clay. J Geotech Eng 120:199–224

42. Yao YP, Wang ND (2014) Transformed stress method for generalizing soil constitutive models. J Eng Mech 140(3):614–629

43. Yu HS (2000) Cavity expansion methods in geomechanics. Kluwer Academic, Dordrecht

44. Zhang J, Li L, Sun DA (2020) Similarity solution for undrained cylindrical cavity contraction in anisotropic modified Cam-clay model soils. Comput Geotech 120:103405

45. Zhuang PZ, Yu HS (2019) Two-dimensional elastoplastic analysis of cylindrical cavity problems in Tresca materials. Int J Num Anal Methods Geomech 43:1612–1633